HHS Public Access

Author manuscript

Cell Rep. Author manuscript; available in PMC 2018 November 27.

Published in final edited form as:

Cell Rep. 2018 October 16; 25(3): 544–550.e3. doi:10.1016/j.celrep.2018.09.052.

Initiation of CNS Myelination in the Optic Nerve Is Dependent on Axon Caliber

Sonia R. Mayoral[1,*], **Ainhoa Etxeberria**[1], **Yun-An A. Shen**[1], and **Jonah R. Chan**[1,2,*]

[1]Department of Neurology, Weill Institute for Neuroscience, University of California, San Francisco, San Francisco, CA 94158, USA

[2]Lead Contact

SUMMARY

Emerging evidence suggests that neuronal signaling is important for oligodendrocyte myelination; however, the necessity of this signaling during development is unclear. By eliminating dynamic neuronal signaling along the developing optic nerve, we find that oligodendrocyte differentiation is not dependent on neuronal signaling and that the initiation of myelination is dependent on a permissive substrate, namely supra-threshold axon caliber. Furthermore, we show that loss of dynamic neuronal signaling results in hypermyelination of axons. We propose that oligodendrocyte differentiation is regulated by non-neuronal factors during optic nerve development, whereas myelination is sensitive to the biophysical properties of axonal diameter.

In Brief

Mayoral et al. show that elimination of neuronal signaling via enucleation of the developing optic nerve of *Wlds* mice results in normal oligodendrocyte differentiation but disrupted myelination. Myelination is rescued when axons are enlarged prior to enucleation, showing that supra-threshold axon caliber, but not neuronal signaling, is necessary for myelination.

Graphical Abstract

*Correspondence: sonia.mayoral@ucsf.edu (S.R.M.), jonah.chan@ucsf.edu (J.R.C.).

AUTHOR CONTRIBUTIONS

S.R.M. and J.R.C. conceived the experiments. S.R.M. and Y.-A.A.S. performed the experiments. S.R.M. and A.E. analyzed the data. S.R.M. and J.R.C. wrote the manuscript.

DECLARATION OF INTERESTS

The authors declare no competing interests.

SUPPLEMENTAL INFORMATION

Supplemental Information includes three figures and can be found with this article online at https://doi.org/10.1016/j.celrep.2018.09.052.

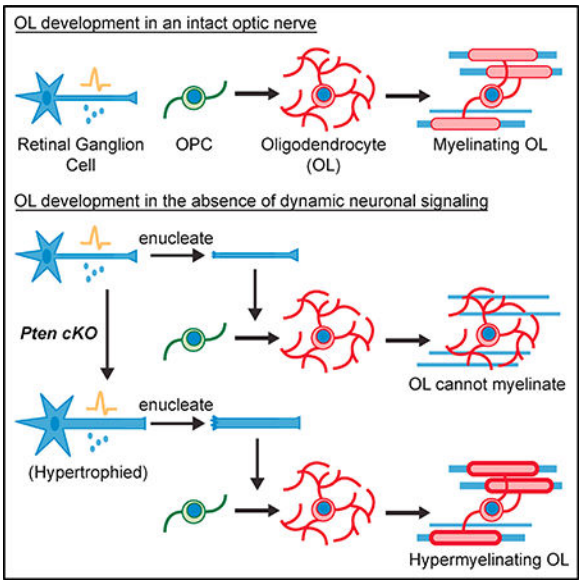

INTRODUCTION

Oligodendrocyte (OL) differentiation and myelination occur in a spatially and temporally stereotyped manner throughout development in the CNS. Notably, the first regions to be occupied by OL precursor cells (OPCs) are not necessarily the first to become myelinated (Colello et al., 1995), suggesting a regulatory role for environmental cues. There is increasing evidence that dynamic neuronal signaling, such as neuronal activity or transcriptional changes, plays a role in regulating these processes (Mitew et al., 2018; Gibson et al., 2014; Mensch et al., 2015; Hines et al., 2015). However, it is unclear whether this signaling is necessary in regions where there is rapid and robust differentiation and myelination, as in the early development of white matter tracts like the optic nerve.

The optic nerve is comprised of axons from retinal ganglion cells (RGCs), whose somas reside within the retina. During development, RGCs exhibit three different stages of activity displayed as spontaneous retinal waves. Stage II waves, which are characterized by relatively infrequent waves, are present from the time of birth in mice and continue through to the second postnatal week (Huberman et al., 2008). The initiation of oligodendrocyte myelination in the optic nerve occurs mid-way through this stage. Because RGC firing is relatively consistent throughout this time, it is difficult to discern how an unchanging firing pattern could convey information about the timing of oligodendrocyte myelination. Rather, a dynamic signal, something that is switched “on” or “off” or undergoes a change just prior to myelination, would be more instructive. We decided to test whether such a dynamic neuronal signal is necessary for the initiation of myelination in the optic nerve.

RESULTS

Enucleation of Postnatal *Wlds* Optic Nerve Disrupts Neuronal Activity

In mice, OPCs begin to migrate into the optic nerve from the brain at birth and proliferate, reaching a maximum density by the end of the first postnatal week (Figure 1A). OPCs begin to differentiate into OLs at 5 days postnatal (P5), and myelination begins at P7 (Figure 1A). If a neuronal signal regulates these distinct processes, that signal would need to be dynamically regulated immediately prior to differentiation and myelination. To test this hypothesis, we eliminated dynamic neuronal signaling, including neuronal activity and transcriptional regulation, at the initiation of myelination and peak of OPC density (P7) by monocular enucleation (EN)—surgically removing one eye, thus leaving behind only transected axons (Ueda et al., 1999; Barres and Raff, 1993; Figure 1B). The remaining eye was left intact to serve as an internal experimental control. To prevent rapid axonal degeneration following transection, we used *Wallerian degeneration* slow (*Wlds*) homozygous mouse mutants, which exhibit delayed axon degeneration (Coleman and Freeman, 2010). We determined that the enucleated axons remain largely intact with minimal overt signs of degeneration up to five days following enucleation (Figure 1C). Because axon initial segments (AISs) are required for initiating action potentials (Kole et al., 2008; Zonta et al., 2011; Kole and Stuart, 2012), removing the somas and AISs of the RGCs will prevent the firing of action potentials along the optic nerve. Although we could not directly measure spontaneous electrical activity of enucleated nerves *in vivo*, we did verify disrupted neuronal activity from the enucleated nerves by examining eye-specific segregation, a correlate of RGC neuronal activity. Forty-eight hours prior to enucleation, cholera toxin B (CTB)-594 was injected into right eyes of mice and CTB-488 was injected into left eyes to label tracts innervating the dorsal lateral geniculate nucleus (dLGN) (Figure 1D). It is well established that the normal pattern of eye-specific segregation of the dLGN (Figure 1D; control mouse) depends on spontaneous neuronal activity of both eyes in early development (Huberman et al., 2008). We observed that enucleation at P7 largely disrupted eye-specific segregation by P10, resulting in increased innervating territory by the left, control eye and overlapping projections from both contralateral and ipsilateral eyes (Figures 1D–1F). These findings are consistent with previous reports of enucleation and neuronal activity inhibition in the optic nerve (Penn et al., 1998; Hayakawa and Kawasaki, 2010; Koch et al., 2011) and suggest that enucleation disrupts neuronal activity in the *Wlds* mutant, despite the overall maintenance of axonal structures.

Elimination of Dynamic Neuronal Signaling Does Not Disrupt OL Differentiation

We first addressed whether dynamic neuronal signaling is necessary for OL differentiation in the optic nerve. To answer this, we immunostained control and enucleated nerves collected at P12, five days after P7 enucleation, with CC1 (mature OLs) and Olig2 (all oligodendroglial lineage cells). We found that, although enucleated nerves were smaller in size at P12 compared to controls due to their lack of growth following transection (Figures S1A and S1B), they had normal densities of both CC1+ OLs and total Olig2+ cells (Figures 2A and 2B). Importantly, the proportional change of differentiated OLs was also normal. CC1+ cell densities increased by two-fold both in control and enucleated nerves from P7 to P12, and the density of Olig2+ oligoden-droglia was unchanged from the time of

enucleation (Figure S1C). Of note, due to a lack of volume increase following enucleation without changes in cell densities, there were fewer Olig2+ and CC1+ cells in P12 enucleated nerves compared to controls (Figure S1D). However, this was not due to cell loss because there were no differences in the numbers of Olig2+ cells in enucleated nerves compared to P7 nerves and there were increased numbers of CC1+ cells in enucleated nerves (Figure S1D). Furthermore, normal CC1+ cell densities were obtained at P5 and they continued to increase through P7 following enucleation at P2 (Figures S2A and S2B), suggesting that the initiation of differentiation was also unaltered. Together, and in line with previous studies (Ueda et al., 1999), these findings demonstrate that dynamic neuronal signaling is not necessary for OL differentiation in the developing optic nerve.

Enucleation Results in Subthreshold Axon Calibers and Disrupted Myelination

To determine whether dynamic neuronal signaling is necessary for myelination, we performed electron microscopic (EM) analysis of control and enucleated P12 nerves. We found that enucleated nerves had substantially fewer numbers of myelinated axons compared to controls (Figures 2C and 2D). This suggested that dynamic neuronal signaling, although not necessary for OL differentiation, may be necessary for myelination. However, it is possible that enucleation not only disrupts dynamic neuronal signaling; it may disrupt a normally permissive environment for myelination. Based on our previous findings concerning suprathreshold (>0.3 μm) fiber diameter as a permissive substrate for myelination (Lee et al., 2012), we analyzed axon diameters at P12. Enucleated nerves had significantly smaller mean axon calibers than controls (Figure 2E), and the majority of axons in enucleated nerves (64%) had diameters under 0.3 μm (Figure 2F). Therefore, it is possible that the lack of myelination observed in enucleated nerves is not due to disrupted neuronal signaling but due to an overwhelming proportion of axons that are not permissive for myelination. To test whether subthreshold axon diameters are responsible for the limited myelination observed following enucleation, we enlarged axon diameters prior to enucleation. Studies have shown that neurons lacking the phosphatase and tensin homolog (PTEN), a negative regulator of the phosphatidylinositol 3-kinase (PI3K)/protein kinase B (AKT)/mammalian target of rapamycin (mTOR) pathway, exhibit axon hypertrophy (Goebbels et al., 2017). We therefore implemented a Cre/ loxP strategy and crossed *Pten* floxed mice to the RGC-specific *Islet1Cre* mouse line (Etxeberria et al., 2016; Elshatory et al., 2007) to obtain RGC-specific *Pten* conditional knockout (cKO) mice. EM analysis of P7 *Pten* floxed control and *Pten* cKO optic nerves revealed that *Pten* cKOs had axon diameters that were on average 32% larger than controls (Figures 2H and 2I). Having successfully increased axon diameters, we crossed the *Pten* cKOs with *Wlds* mutants and repeated the enucleation experiments.

Increasing Axon Calibers Rescues Myelination Defect and Reveals Hypermyelination

Similar to *Wlds* nerves, enucleated *Wlds Pten* cKO nerves showed no differences in Olig2+ and CC1+ cell densities compared to controls (Figures 3A and 3B); thus, OL differentiation was again not affected by loss of dynamic neuronal signaling. Strikingly, EM analysis of myelination revealed that, unlike enucleated *Wlds* nerves, which had decreased myelination, enucleated *Wlds Pten* cKO nerves had a normal percentage of myelinated axons compared to controls (Figures 3C and 3D). Analysis of axon diameters revealed that enucleated *Wlds*

Pten cKO axon diameters were still smaller than control nerves but that the majority of axons (60%) had diameters above 0.3 mm (Figures 3E and 3F). Therefore, increasing axon diameters was sufficient to rescue the myelination deficit. Examination of astrocytes in control and enucleated nerves via GFAP immunostaining revealed no differences following enucleation in *Wlds* or *Wlds Pten* cKOs (Figures S3A and S3B). Also examination of microglia via Iba1 immunostaining showed an expected injury-induced increase in microglial cell densities in both *Wlds* and *Wlds Pten* cKOs (Figures S3C and S3D). Together, these data indicate that dynamic neuronal signaling is not necessary for myelination in the early development of the optic nerve. Furthermore, g-ratio analysis, a measure of myelin thickness, revealed that enucleated axons had smaller g-ratios and thus thicker myelin versus controls (Figure 3G). This difference was significant in axons as large as 1.5 mm (Figure 3H). Examining the g-ratios in enucleated *Wlds* nerves showed similar results (Figure 2G). This finding, although surprising, seems to suggest that there is a mechanism that limits the number of wraps of myelin and that this mechanism may be dependent on dynamic neuronal signaling. Alternatively, it may suggest that the mechanism for regulating g-ratios takes into account initial axon calibers and integrates the future growth of axon diameters throughout development, and because enucleated axons cannot grow, they become excessively myelinated.

DISCUSSION

Our findings indicate that dynamic neuronal signaling is not necessary for OL differentiation and myelination in the developing optic nerve. We propose that, during development, axon diameters increase to reach a permissive size (>0.3 mm) for myelination to occur and, upon differentiation, OLs will myelinate permissive axons. However, unlike the optic nerve, which becomes completely myelinated, most other brain regions are only partially myelinated, even though many axons in those regions are permissive in size. Therefore, it is likely that axons in these other regions express inhibitory or repulsive signals (Redmond et al., 2016) that prevent myelination from occurring. Because myelination cannot occur without OL differentiation, it is also possible that certain microenvironmental signals could inhibit OPCs from differentiating or, conversely, that there exists a lack of differentiation-promoting cues. Moreover, attractive cues could also exist that help dictate which axonal regions become myelinated, although none have yet been discovered. A lack of attraction could also result in a lack of myelination around certain axons and perhaps lead to more stochastic patterns of myelination; however, it is most likely that many, if not all, of these signals exist to guide OL myelination throughout the brain (Osso and Chan, 2017). It is important to note that, during development, myelination will occur, regardless of external stimuli or experience given a permissive environment. Studies using dark rearing and ocular deprivation find that normal levels of myelination develop within optic nerves (Moore et al., 1976; Etxeberria et al., 2016). However, external stimuli and experiential changes will affect myelination largely through activity-dependent processes (Makinodan et al., 2012; McKenzie et al., 2014; Gibson et al., 2014; Mitew et al., 2018; Purger et al., 2016). Still, this adaptive myelination seems to be dependent on a permissive environment set forth by supra-threshold axon diameters, as myelinated axons below 0.3 mm are rarely found *in vivo*.

Previous studies have attempted to test whether neuronal signaling is necessary for myelination in the optic nerve. Ueda et al. (1999) similarly performed enucleations to disrupt dynamic neuronal signaling, but in rats instead of *Wlds* mice. Consistent with our findings, they found that OLs developed normally in enucleated nerves. It is important to note that they could not assess myelination effects, because axons completely degenerated, but claimed that axons were required for the increased number of OL processes and process length seen in intact nerves. Whether the axon structure itself or dynamic axonal signaling was required for these increases was not addressed. In a different study, Demerens et al. (1996) blocked neuronal activity in the developing optic nerve by injecting TTX into the eyes of P4 mouse pups and showed a decrease in myelinated axons two days later at P6 despite no differences in OL numbers. Although a direct effect of TTX on OPCs and OLs cannot be ruled out, it is possible that the loss of neuronal activity also slowed axon growth because recent studies have shown that neuronal activity can increase axon size (Chéreau et al., 2017; Sinclair et al., 2017). Interestingly, there was no effect of TTX on myelination if the injections were performed one day later at P5, perhaps because the extra time allowed for sufficient axon growth or more likely blocking action potentials has minimal effects on optic nerve myelination because no changes in myelination were seen when TTX was injected into rat pup eyes daily from P0 to P9 in a different study by Colello et al., (1995).

Although the requirement of supra-threshold calibers for myelination to occur was uncovered in our previously published work in vitro (Lee et al., 2012), our current work clearly demonstrates this requirement *in vivo*. A recent study by Goebbels et al. (2017) also increased axon diameters by conditionally removing *Pten* and strikingly showed that myelination could be observed around the normally unmyelinated axons of cerebellar granule cells. However, they could not separate out the effects of transcriptional changes in neurons from changes in axon calibers, and so it remained unclear what the ectopic myelination was due to. Furthermore, by examining a region normally devoid of OLs, it was not clear whether the recruitment and differentiation of OPCs alone could produce this effect. By focusing on the optic nerve, a region highly populated by OPCs and OLs, and by removing the transcriptional machinery of RGCs via enucleation, we were able to tease these variables apart and reveal the effects of changing axon calibers.

Our work suggests that fiber diameter alone allows myelination to initiate, but it still remains unknown how OLs sense the biophysical property of axon caliber. However, we can speculate that neuronal signaling plays specific roles in OPC proliferation and g-ratio control. Additionally, we suggest that non-neuronal factors trigger OL differentiation. There is already growing evidence of vascular, astroglial, and microglial regulators of OL differentiation. Yuen et al. (2014) showed that hypoxia from lack of brain vascularization early on in development can inhibit OPCs from differentiating. Astrocytes are known to secrete factors, including chondroitin sulfate proteoglycans (CSPGs), that have been shown to inhibit OL differentiation and myelination in CNS lesions (Harlow and Macklin, 2014). Similarly, microglia have been shown to affect OPC differentiation after CNS injury, as Miron et al. (2013) showed that anti-inflammatory M2 microglia may help to drive OPC differentiation via the release of activin-A during remyelination. Although these latter roles of astrocytes and microglia have only been shown in response to injury, it is possible that

they or similar factors may also play a role in inhibiting or promoting, respectively, OPC differentiation during development.

It is increasingly clear that CNS myelination can be modulated by an array of neuronal factors (Klingseisen and Lyons, 2018; Osso and Chan, 2017). However, our findings provide insight into the minimal requirements harnessed by the CNS to efficiently myelinate the optic nerve during early development. Further studies are required to determine what factors control OL differentiation in white and gray matter, whether the mechanisms are similar, and what constitutes a permissive substrate for membrane wrapping in other areas of the CNS that require prolonged myelination and plasticity.

STAR⋆METHODS

KEY RESOURCES TABLE

REAGENT or RESOURCE	SOURCE	IDENTIFIER
Antibodies		
rabbit anti-PDGFRα	W.B. Stallcup, Sanford Burnham Prebys Medical Discovery Institute, La Jolla, CA	N/A
mouse anti-CC1	Calbiochem	Cat: OP80; RRID: AB_2057371
rabbit anti-Olig2	Millipore	Cat: AB9610; RRID: AB_570666
mouse anti-Neurofilament	Covance	Cat: SMI-312R-100; RRID: AB_2314906
mouse anti-GFAP	EMD Millipore	Cat: MAB360; RRID: AB_11212597
rabbit anti-Iba1	Wako	Cat: 019–19741; RRID: AB_839504
rabbit anti-*WLDS*	Abcam	Cat: ab94345; RRID: AB_10672212
Alexa Fluor 488 goat anti-rabbit IgG	Life Technologies	Cat: A-11008; RRID: AB_143165
Alexa Fluor 488 goat anti-mouse IgG	Life Technologies	Cat: A-11029; RRID: AB_138404
Alexa Fluor 594 goat anti-rabbit IgG	Life Technologies	Cat: A-11037; RRID: AB_2534095
Alexa Fluor 594 goat anti-mouse IgG	Life Technologies	Cat: A-11005; RRID: AB_141372
Alexa Fluor 647 goat anti-rabbit IgG	Life Technologies	Cat: A-21245; RRID: AB_141775
Alexa Fluor 647 goat anti-mouse IgG	Life Technologies	Cat: A-21236; RRID: AB_141725
Chemicals, Peptides, and Recombinant Proteins		
Cholera toxin B 594	Invitrogen	Cat: C22842
Cholera toxin B 488	Invitrogen	Cat: C34775
Experimental Models: organisms/strains		
Mouse: *Wlds*: FVB.B-*Wlds*/UmonJ	Jackson Laboratory	Cat: 008820; RRID: IMSR_JAX:008820
Mouse: *Pten* fl/fl: B6.129S4-*Pten*tm1Hwu/J	Jackson Laboratory	Cat: 006440; RRID: IMSR_JAX:006440
Mouse: *Islet1*Cre: Isl1tm1(cre)Sev/J	Jackson Laboratory	Cat: 024242; RRID: IMSR_JAX:024242
Software and Algorithms		
ImageJ	NIH	https://imagej.nih.gov/ij/; RRID: SCR_003070
AxioVision 4	Zeiss	https://www.zeiss.com/microscopy/int/products/microscope-software/axiovision.html; RRID: SCR_002677
Adobe Photoshop CS5.1	Adobe	RRID: SCR_014199
Microsoft Excel 2011	Microsoft	RRID: SCR_016137

REAGENT or RESOURCE	SOURCE	IDENTIFIER
Prism 5	Graphpad	RRID: SCR_002798
FIJI	NIH	https://fiji.sc/; RRID: SCR_002285

CONTACT FOR REAGENT AND RESOURCE SHARING

Further information and requests for reagents and resources should be directed to and will be fulfilled by the Lead Contact, Jonah Chan (jonah.chan@ucsf.edu).

EXPERIMENTAL MODEL AND SUBJECT DETAILS

Animals

All mice were handled in accordance with the approval of the University of California San Francisco Administrative Panel on Laboratory Animal Care and housed under standard, barrier conditions in the Laboratory Animal Research Center (LARC) in the Sandler Neurosciences Center at UCSF, Mission Bay. *Wlds* mice, previously described by Kariya et al. (Kariya et al., 2009) and Lyon et al. (Lyon et al., 1993), were purchased from the Jackson Laboratory (Stock No: 008820) as heterozygotes. These were bred to obtain homozygous mice and only homozygous *Wlds* mouse pups from P2-P14 were used in experiments. *Pten* fl/fl mice (Jackson Laboratory, Stock No: 006440), previously described by Lesche et al. (Lesche et al., 2002), were crossed to *Islet1*Cre ± mice (Jackson Laboratory, Stock No: 024242), previously described by Yang et al. (Yang et al., 2006), to generate *Islet1*Cre ±; *Pten* fl/+ heterozygotes. These mice were bred to *Pten* fl/fl mice to obtain conditional knock-out (cKO) homozygous mice (*Islet1*Cre ±; *Pten* fl/fl) and littermate controls (*Pten* fl/fl). Additionally, *Islet1*Cre; *Pten* fl/fl mice were crossed with *Wlds* mice to first obtain *Islet1*Cre ±; *Pten* fl/+; *Wlds* ± heterozygotes. These were crossed with *Pten* fl/+; *Wlds* ± littermates to obtain *Islet1* conditional, *Pten* floxed homozygotes and littermate controls on a homozygous *Wlds* background (*Wlds*; *Islet1*Cre ±; *Pten* fl/fl and *Wlds*; *Pten* fl/fl, respectively), which were used in experiments and only postnatal pups from P7-P12 were used. Genotypes of *Pten* floxed mice and *Islet1*Cre mice were determined by standard PCR analysis of toe genomic DNA using appropriate primers and parameters found on The Jackson Laboratory website, while genotypes of *Wlds* mice were determined by qPCR analysis of tail or toe genomic DNA using previously described methods (Wishart et al., 2007) and confirmed by standard western blot analysis of tail tissue using a rabbit anti-*WLDS* antibody (Abcam, Cat #ab94345). Since wild-type mice produce no *WLDS* protein they exhibit no bands. Heterozygous *Wlds* mice produce half as much *WLDS* protein as homozygous mice and so the two can be differentiated by the intensity of the *WLDS* protein bands. Male and female mice were used for all experiments without bias.

METHOD DETAILS

Enucleation surgery

Postnatal day 2 or 7 pups were cryoanesthetized on ice and then positioned under a dissecting scope so that the right eye was facing up. Following alcohol and betadine disinfection of the eye area, the margins of the closed eye were separated using sharp

forceps. Proparacaine hydrochloride ophthalmic solution (0.5%; Akorn, NDC #17478–263-12) was then dropped into the open eye for local anesthesia. Blunt, bent forceps were pressed down around the eye to briefly pop the eye out from the socket and the entire eye was immediately removed using curved scissors. Subsequent bleeding was cauterized using silver nitrate applicators (Grafco, NDC #12165–100-03). Finally, the pups were placed on a warming pad to recover. Once recovered, the pups were placed back into their home cages.

Cholera toxin B (CTB) labeling

Postnatal day 5 pups were cryoanesthetized on ice and then positioned under a dissecting scope so that one eye was facing up. Following alcohol and betadine disinfection of the eye area, the margins of the closed eye were separated using sharp forceps. Proparacaine hydrochloride ophthalmic solution (0.5%; Akorn, NDC #17478–263-12) was then dropped into the open eye for local anesthesia. A 30-gauge needle was used to puncture a hole through the eye into the vitreous. A Kimwipe was used to absorb some of the vitreous solution through the puncture. One microliter of CTB-594 (right eye; Invitrogen, Cat #C22842) or CTB-488 (left eye; Invitrogen, Cat #C34775) was then slowly injected intravitreally through the puncture over 1 minute using a pulled glass pipet. The pipet was held in place for a minute longer immediately following the injection. Neomycin-Polymyxin B-Dexamethasone ophthalmic antibiotic ointment (Bausch+Lomb, NDC #24208–795-35) was then placed directly over the puncture to prevent infection and help seal the hole. Pups were then repositioned on their opposite side and the entire procedure was repeated for the other eye. After both eyes were injected, the pups were placed on a warming pad to recover and then placed back into their home cages. Pups were randomly assigned to be enucleated or left intact two days later. At P10 pups were decapitated and their brains were placed into 4% paraformaldehyde for overnight fixation at 4°C. Brains were then transferred to 30% sucrose and allowed to sink at 4°C for 2 days for cryoprotection. Brains were cryosectioned coronally to 50μm thickness using a sliding microtome (Microm HM450) with a freezing stage (Microm KS34) and sections containing dLGN were collected, rinsed in PBS, and mounted onto Superfrost Plus microscope slides. After drying, the slides were coverslipped using Glycergel mounting medium (Dako, Cat #C056330) for imaging.

Immunofluorescence staining

Postnatal day 5, 7, or 12 pups were quickly decapitated and optic nerves were freshly dissected out then immediately placed into cold 4% paraformaldehyde for overnight fixation at 4°C. Nerves were then transferred to 30% sucrose for cryoprotection. After the nerves sunk into the sucrose (24 hr at 4°C) the nerves were cryosectioned longitudinally to 30μm thickness using a sliding microtome (Microm HM450) with a freezing stage (Microm KS34). Floating sections were washed in PBS then blocked and permeablized in 10% normal goat serum (NGS) + 0.2% Triton X-100 for 1 hr at RT. Sections were then incubated in primary antibodies diluted in blocking solution overnight at 4°C. Primary antibodies and their dilutions were as follows: rabbit polyclonal antibody to PDGFRα (1:8000; gift from W. B. Stallcup, Sanford Burnham Prebys Medical Discovery Institute, La Jolla, CA), rabbit polyclonal antibody to Olig2 (1:1000; Millipore, Cat #AB9610), mouse monoclonal antibody to CC1 (1:1000, Calbiochem, Cat #OP80), mouse monoclonal antibody to neurofilament (1:2000, Covance, Cat #SMI-312R-100), mouse monoclonal antibody to

GFAP (1:1000, EMD Millipore, Cat #MAB360), rabbit polyclonal antibody to Iba1 (1:1000, Wako, Cat #019–19741). Sections were then washed in PBS for 1 hr at RT and then incubated in secondary antibodies diluted in 10% NGS + DAPI (20ng/ml; Invitrogen, Cat #D1306) for 2 hr at RT. Secondary antibodies and their dilutions are as follows: AlexaFluor 488-, AlexaFluor 594-, and AlexaFluor 647-conjugated goat antibodies to rabbit or mouse (1:1000; Invitrogen). Sections were washed in PBS, rinsed briefly in distilled water, and mounted onto Superfrost Plus microscope slides to dry. When completely dry the slides were coverslipped using Glycergel mounting medium (Dako, Cat #C056330) for imaging.

Electron microscopy (EM)

Postnatal day 7 or 12 pups were quickly decapitated and optic nerves were freshly dissected out then immediately placed into 2% paraformaldehyde/1.25% glutaraldehyde in 0.1M sodium cacodylate buffer for fixation at 4°C. Further processing and TEM imaging was carried out by the Gladstone EM core facility. Briefly, tissue was postfixed in 2% osmium tetroxide in 0.1M sodium cacodylate buffer, then stained with 2% aqueous uranyl acetate, dehydrated in acetone, infiltrated, and embedded in LX-112 resin (Ladd Research Industries). Samples were then ultrathin sectioned transversely on a Reichert Ultracut S ultramicrotome and counterstained with 0.8% lead citrate. Grids were examined on a JEOL JEM-1230 transmission electron microscope and photographed with the Gatan Ultrascan 1000 digital camera.

QUANTIFICATION AND STATISTICAL ANALYSIS

Image analysis

Immunofluorescent images were acquired on a Zeiss Axio Imager Z1 fluorescence microscope with Apotome using AxioVision software. Maximal intensity projections from acquired z stacks through the entire section were then analyzed using ImageJ software (NIH). Cell densities were obtained by counting positively stained cells in three representative 20X fields from each section and dividing by the volume of each section per field. Volumes were obtained by measuring the area of each section per field and multiplying by the section thickness. Optic nerve diameters were calculated by dividing the area of the nerve from these same 20× images by the length of the nerve to obtain the widths (diameters) of the nerves. ImageJ software (NIH) was also used to obtain axon diameter measurements (feret diameter) from EM images taken at 4000X magnification (≥ 904 axons measured per group) and g-ratios from EM images taken at 1500X magnification (≥ 136 axons measured per group) using the freehand selection tool. For g-ratios the inner myelin sheath diameter was divided by the outer myelin sheath diameter. The percentage of myelinated axons was manually counted from EM images taken at 1500X (≥ 1501 axons counted per group). For CTB image analysis, 10X images of fluorescently labeled dLGN were opened in Adobe Photoshop, manually thresholded, and then corresponding images of each dLGN were multiplied. Multiplied images were opened in FIJI (NIH), cropped to exclude regions outside of the dLGN, and then the create selection tool was used to select ipsilateral, contralateral, and overlapping projection regions in the dLGN as well as the entire dLGN. The areas of these regions were then measured to obtain the percentages of

ipsilateral territory and overlap. Two or more dLGN-containing sections were used from each animal for measurements of each dLGN.

Statistical analysis

Statistical analyses were performed on Excel using two-tailed Student's t test, for all comparisons except those in Figures 3H and S1, which were analyzed using a one-way ANOVA with Bonferroni posttests on Prism software, to determine statistical significance that is expressed as *$p < 0.05$, **$p < 0.01$, or ***$p < 0.001$. N values represent numbers of optic nerves or mice (CTB analysis) measured per group.

Supplementary Material

Refer to Web version on PubMed Central for supplementary material.

ACKNOWLEDGMENTS

We would like to thank all of the members of the Chan laboratory for their helpful review of the manuscript and insightful comments. We would also like to thank S.Y. Chew and J.S. Chin for their contributions not included in this manuscript, as well as E.M. Ullian and A.V. Molofsky for their expert advice. S.R.M. would like to thank G.R. Mayoral and E.S. Arroyo for their support. This work was funded by the NIH/NINDS (R01NS062796, R01NS097428, and R01NS095889), The Adelson Medical Research Foundation (A130141), and the Rachleff family endowment to J.R.C. and the NIH/NIGMS IRACDA postdoctoral fellowship (K12GM081266) and the NIH/NINDS career transition award (K22NS104234) to S.R.M.

REFERENCES

Barres BA, and Raff MC (1993). Proliferation of oligodendrocyte precursor cells depends on electrical activity in axons. Nature 361, 258–260. [PubMed: 8093806]

Che´ reau R, Saraceno GE, Angibaud J, Cattaert D, and Na¨ gerl UV (2017). Superresolution imaging reveals activity-dependent plasticity of axon morphology linked to changes in action potential conduction velocity. Proc. Natl. Acad. Sci. USA 114, 1401–1406. [PubMed: 28115721]

Colello RJ, Devey LR, Imperato E, and Pott U (1995). The chronology of oligodendrocyte differentiation in the rat optic nerve: evidence for a signaling step initiating myelination in the CNS. J. Neurosci 15, 7665–7672. [PubMed: 7472517]

Coleman MP, and Freeman MR (2010). Wallerian degeneration, wld(s), and nmnat. Annu. Rev. Neurosci 33, 245–267. [PubMed: 20345246]

Demerens C, Stankoff B, Logak M, Anglade P, Allinquant B, Couraud F, Zalc B, and Lubetzki C (1996). Induction of myelination in the central nervous system by electrical activity. Proc. Natl. Acad. Sci. USA 93, 9887–9892. [PubMed: 8790426]

Elshatory Y, Deng M, Xie X, and Gan L (2007). Expression of the LIMhomeodomain protein Isl1 in the developing and mature mouse retina. J. Comp. Neurol 503, 182–197. [PubMed: 17480014]

Etxeberria A, Hokanson KC, Dao DQ, Mayoral SR, Mei F, Redmond SA, Ullian EM, and Chan JR (2016). Dynamic modulation of myelination in response to visual stimuli alters optic nerve conduction velocity. J. Neurosci 36, 6937–6948. [PubMed: 27358452]

Gibson EM, Purger D, Mount CW, Goldstein AK, Lin GL, Wood LS, Inema I, Miller SE, Bieri G, Zuchero JB, et al. (2014). Neuronal activity promotes oligodendrogenesis and adaptive myelination in the mammalian brain. Science 344, 1252304. [PubMed: 24727982]

Goebbels S, Wieser GL, Pieper A, Spitzer S, Weege B, Yan K, Edgar JM, Yagensky O, Wichert SP, Agarwal A, et al. (2017). A neuronal PI(3,4,5)P3-dependent program of oligodendrocyte precursor recruitment and myelination. Nat. Neurosci 20, 10–15. [PubMed: 27775720]

Harlow DE, and Macklin WB (2014). Inhibitors of myelination: ECM changes, CSPGs and PTPs. Exp. Neurol 251, 39–46. [PubMed: 24200549]

Hayakawa I, and Kawasaki H (2010). Rearrangement of retinogeniculate projection patterns after eye-specific segregation in mice. PLoS One 5, e11001. [PubMed: 20544023]

Hines JH, Ravanelli AM, Schwindt R, Scott EK, and Appel B (2015). Neuronal activity biases axon selection for myelination *in vivo*. Nat. Neurosci 18, 683–689. [PubMed: 25849987]

Huberman AD, Feller MB, and Chapman B (2008). Mechanisms underlying development of visual maps and receptive fields. Annu. Rev. Neurosci 31, 479–509. [PubMed: 18558864]

Kariya S, Mauricio R, Dai Y, and Monani UR (2009). The neuroprotective factor Wld(s) fails to mitigate distal axonal and neuromuscular junction (NMJ) defects in mouse models of spinal muscular atrophy. Neurosci. Lett 449, 246–251. [PubMed: 19010394]

Klingseisen A, and Lyons DA (2018). Axonal regulation of central nervous system myelination: structure and function. Neuroscientist 24, 7–21. [PubMed: 28397586]

Koch SM, Dela Cruz CG, Hnasko TS, Edwards RH, Huberman AD, and Ullian EM (2011). Pathway-specific genetic attenuation of glutamate release alters select features of competition-based visual circuit refinement. Neuron 71, 235–242. [PubMed: 21791283]

Kole MHP, and Stuart GJ (2012). Signal processing in the axon initial segment. Neuron 73, 235–247. [PubMed: 22284179]

Kole MHP, Ilschner SU, Kampa BM, Williams SR, Ruben PC, and Stuart GJ (2008). Action potential generation requires a high sodium channel density in the axon initial segment. Nat. Neurosci 11, 178–186. [PubMed: 18204443]

Lee S, Leach MK, Redmond SA, Chong SY, Mellon SH, Tuck SJ, Feng ZQ, Corey JM, and Chan JR (2012). A culture system to study oligodendrocyte myelination processes using engineered nanofibers. Nat. Methods 9, 917–922. [PubMed: 22796663]

Lesche R, Groszer M, Gao J, Wang Y, Messing A, Sun H, Liu X, and Wu H (2002). Cre/loxP-mediated inactivation of the murine *Pten* tumor suppressor gene. Genesis 32, 148–149. [PubMed: 11857804]

Lyon MF, Ogunkolade BW, Brown MC, Atherton DJ, and Perry VH (1993). A gene affecting Wallerian nerve degeneration maps distally on mouse chromosome 4. Proc. Natl. Acad. Sci. USA 90, 9717–9720. [PubMed: 8415768]

Makinodan M, Rosen KM, Ito S, and Corfas G (2012). A critical period for social experience-dependent oligodendrocyte maturation and myelination. Science 337, 1357–1360. [PubMed: 22984073]

McKenzie IA, Ohayon D, Li H, de Faria JP, Emery B, Tohyama K, and Richardson WD (2014). Motor skill learning requires active central myelination. Science 346, 318–322. [PubMed: 25324381]

Mensch S, Baraban M, Almeida R, Czopka T, Ausborn J, El Manira A, and Lyons DA (2015). Synaptic vesicle release regulates myelin sheath number of individual oligodendrocytes *in vivo*. Nat. Neurosci 18, 628–630. [PubMed: 25849985]

Miron VE, Boyd A, Zhao JW, Yuen TJ, Ruckh JM, Shadrach JL, van Wijngaarden P, Wagers AJ, Williams A, Franklin RJM, and FfrenchConstant C (2013). M2 microglia and macrophages drive oligodendrocyte differentiation during CNS remyelination. Nat. Neurosci 16, 1211–1218. [PubMed: 23872599]

Mitew S, Gobius I, Fenlon LR, McDougall SJ, Hawkes D, Xing YL, Bujalka H, Gundlach AL, Richards LJ, Kilpatrick TJ, et al. (2018). Pharmacogenetic stimulation of neuronal activity increases myelination in an axon-specific manner. Nat. Commun 9, 306. [PubMed: 29358753]

Moore CL, Kalil R, and Richards W (1976). Development of myelination in optic tract of the cat. J. Comp. Neurol 165, 125–136. [PubMed: 1245609]

Osso LA, and Chan JR (2017). Architecting the myelin landscape. Curr. Opin. Neurobiol 47, 1–7. [PubMed: 28709021]

Penn AA, Riquelme PA, Feller MB, and Shatz CJ (1998). Competition in retinogeniculate patterning driven by spontaneous activity. Science 279, 2108–2112. [PubMed: 9516112]

Purger D, Gibson EM, and Monje M (2016). Myelin plasticity in the central nervous system. Neuropharmacology 110 (Pt B), 563–573. [PubMed: 26282119]

Redmond SA, Mei F, Eshed-Eisenbach Y, Osso LA, Leshkowitz D, Shen YA, Kay JN, Aurrand-Lions M, Lyons DA, Peles E, and Chan JR (2016). Somatodendritic expression of JAM2 inhibits oligodendrocyte myelination. Neuron 91, 824–836. [PubMed: 27499083]

Sinclair JL, Fischl MJ, Alexandrova O, Heb M, Grothe B, Leibold C, and Kopp-Scheinpflug C (2017). Sound-evoked activity influences myelination of brainstem axons in the trapezoid body. J. Neurosci 37, 8239–8255. [PubMed: 28760859]

Ueda H, Levine JM, Miller RH, and Trapp BD (1999). Rat optic nerve oligodendrocytes develop in the absence of viable retinal ganglion cell axons. J. Cell Biol 146, 1365–1374. [PubMed: 10491397]

Wishart TM, Macdonald SH, Chen PE, Shipston MJ, Coleman MP, Gillingwater TH, and Ribchester RR (2007). Design of a novel quantitative PCR (QPCR)-based protocol for genotyping mice carrying the neuroprotective Wallerian degeneration slow (*Wlds*) gene. Mol. Neurodegener 2, 21. [PubMed: 17971231]

Yang L, Cai CL, Lin L, Qyang Y, Chung C, Monteiro RM, Mummery CL, Fishman GI, Cogen A, and Evans S (2006). Isl1Cre reveals a common Bmp pathway in heart and limb development. Development 133, 1575–1585. [PubMed: 16556916]

Yuen TJ, Silbereis JC, Griveau A, Chang SM, Daneman R, Fancy SPJ, Zahed H, Maltepe E, and Rowitch DH (2014). Oligodendrocyteencoded HIF function couples postnatal myelination and white matter angiogenesis. Cell 158, 383–396. [PubMed: 25018103]

Zonta B, Desmazieres A, Rinaldi A, Tait S, Sherman DL, Nolan MF, and Brophy PJ (2011). A critical role for Neurofascin in regulating action potential initiation through maintenance of the axon initial segment. Neuron 69, 945–956. [PubMed: 21382554]

Highlights

- Oligodendrocyte differentiation is not dependent on dynamic neuronal signals
- Supra-threshold axon caliber is necessary for myelination *in vivo*
- Dynamic neuronal signaling in not necessary for oligodendrocyte myelination
- Neuronal signaling may be required for limiting myelin wraps

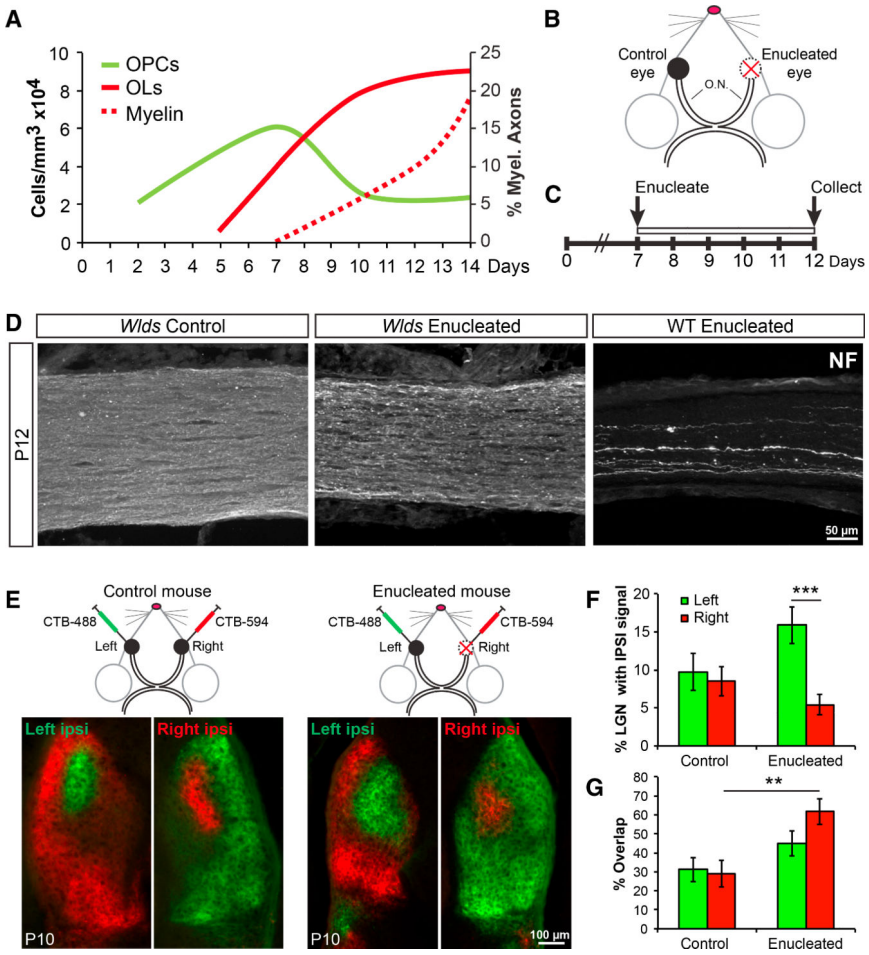

Figure 1. Enucleation of *Wlds* Optic Nerves Eliminates Dynamic Neuronal Signaling

(A) Timeline of early OL development in the mouseoptic nerve. Measurements were collected from immunostaining of optic nerves for PDGFRα+ OPCs (green) and CC1+ OLs (solid red), as well as EM analysis for myelinated axons (dashed red) at various time points from P2 to P14.

(B) Illustration of monocular enucleation strategy.Right eyes were enucleated, and left eyes were left intact to serve as controls. O.N., optic nerves.

(C) Timeline for experiment showing enucleation at P7 and collection of optic nerves at P12.

(D) Neurofilament (NF) staining of optic nerves5 days after enucleation. Axons of *Wlds* enucleated nerves (middle) appear intact versus wildtype (WT) enucleated nerves (right). Control nerve is on the left.

(E) Schematic of CTB injection strategy and representative images are of dLGN staining at P10.

(F) Quantification of the percentage of dLGN with ipsilateral signal shows a large increase in the territory occupied by the control eye of enucleated mice. N = 5.

(G) Quantification of the percent ipsilateral signal that overlaps with contralateral signal in the dLGN shows significantly more overlap in the enucleated ipsilateral territory. N = 5–12. **p < 0.01; ***p < 0.001. Error bars represent ±SEM.

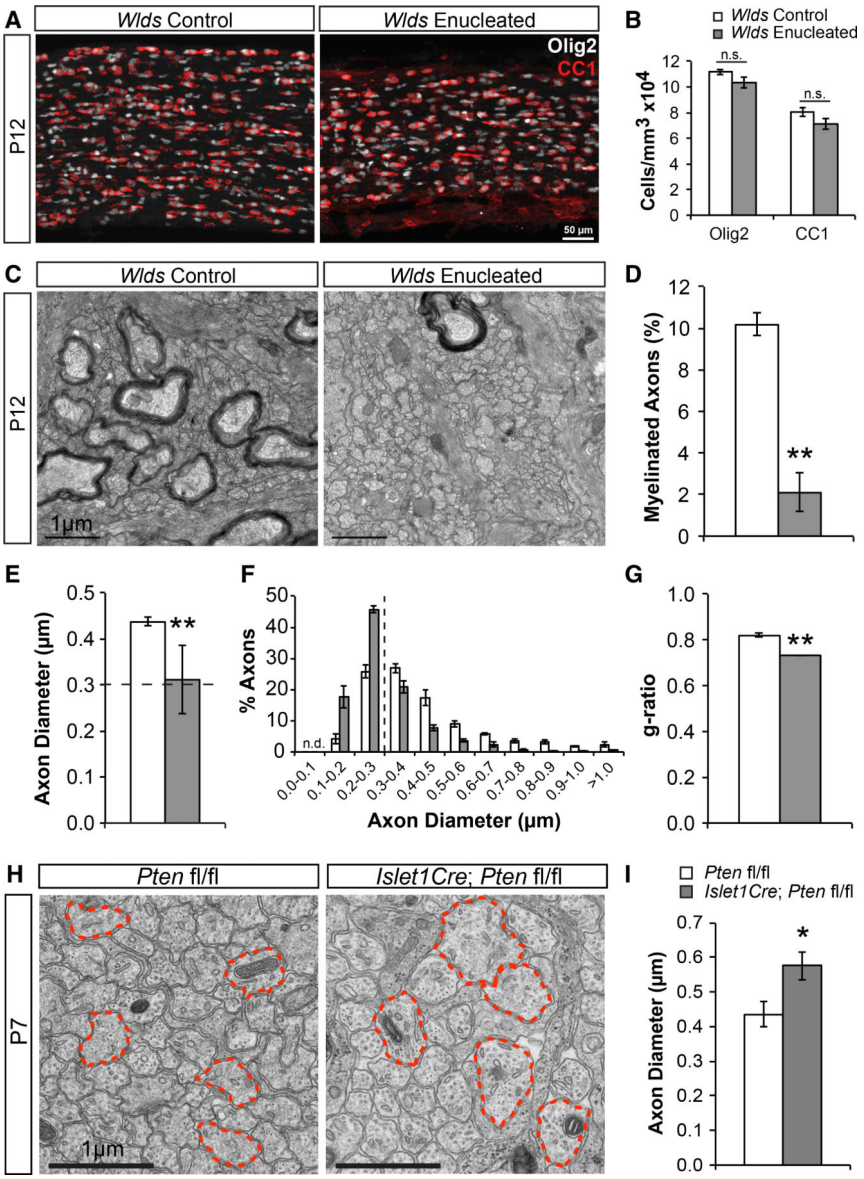

Figure 2. Enucleated Optic Nerves Exhibit Normal OL Differentiation but Disrupted Myelination

(A) *Wlds* control and enucleated optic nerves stained for oligodendroglia (Olig2; white) and mature OLs (CC1; red).

(B) Quantification of Olig2 and CC1 cell densitiesshows no differences between groups. N = 15–17.

(C) Electron microscopy (EM) images of *Wlds* control and enucleated optic nerves.

(D) Quantification of the percentage of myelinated axons shows a significant reduction of myelinated axons in enucleated nerves. N = 3.

(E) Quantification of axon diameters shows a significant reduction of axon diameters in enucleated nerves. Dashed line represents 0.3 mm threshold. N = 3.

(F) Quantification of the percentage of axonsfound at each diameter range shown. The majority of enucleated axons (64%) are found below 0.3 mm (dashed line), compared to only 30% of control axons. N = 3.

(G) Quantification of g-ratios shows significantlylower g-ratios in enucleated nerves representing thicker myelin. N = 3.

(H) EM images of control (*Pten* fl/fl) and RGC-specific *Pten* cKO (*Islet1Cre*; *Pten* fl/fl) optic nerves. Red outlines highlight the largest axons in the field.

(I) Quantification of axon diameters shows significantly increased diameters in *Pten* cKOs. N = 4. n.s., not significant; *p < 0.05; **p < 0.01. Error bars represent ±SEM. See also Figures S1, S2, and S3.

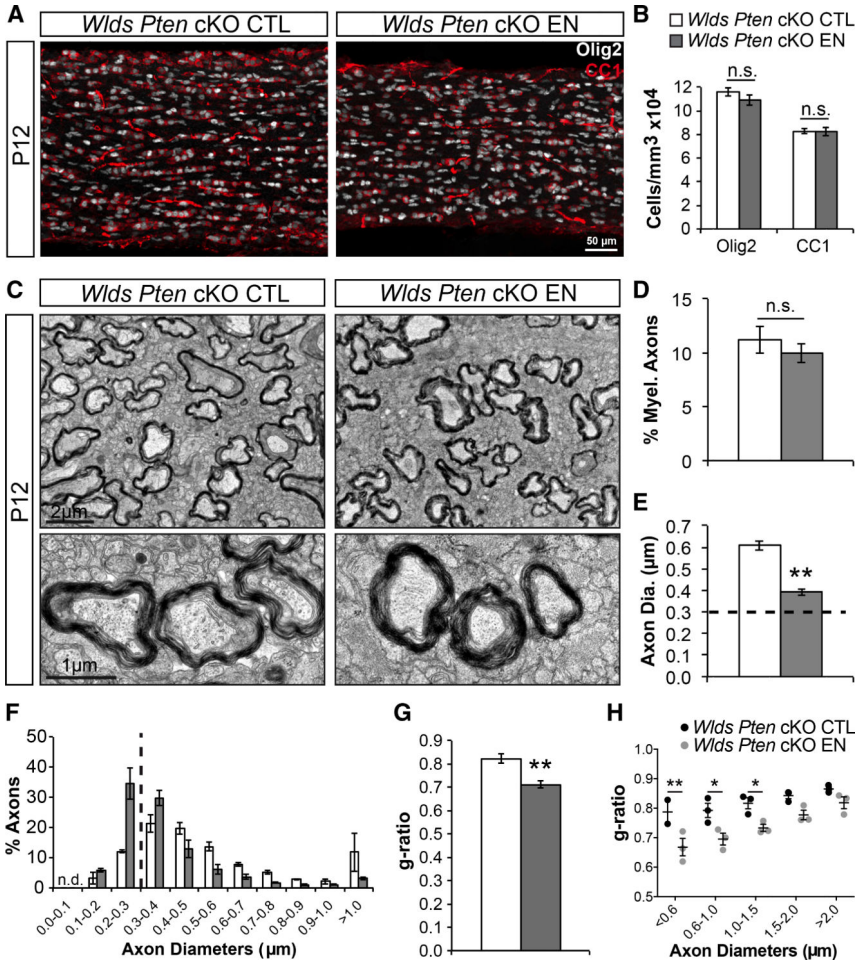

Figure 3. Increasing Axon Diameters Rescues Myelination Deficit in Enucleated Optic Nerves

(A) *Wlds Pten* cKO control (CTL) and enucleated (EN) optic nerves stained for Olig2 (white) and CC1 (red).

(B) Quantification of Olig2 and CC1 cell densitiesshows no differences between groups. N = 13–15.

(C) EM images of CTL and EN *Wlds Pten* cKO optic nerves.

(D) Quantification of the percentage of myelinated axons shows no differences between groups.N = 3.

(E) Quantification of axon diameters continuesto show reduced diameters in enucleated nerves, but the average is well above 0.3 mm (dashed line). N = 3.

(F) Quantification of the percentage of axons found at each diameter range shown. The majority of enucleated axons (60%) are now above 0.3 µm.N = 3.

(G) Quantification of g-ratios continues to show significantly lower g-ratios in enucleated nerves. N = 3.

(H) Scatterplot of mean g-ratios by axon diameter shows that enucleated axons below 1.5 mm have significantly smaller g-ratios. N = 3.

*p < 0.05; **p < 0.01. Error bars represent ±SEM. See also Figure S3.